Earth and Planetary Science Letters 364 (2013) 68–84

Contents lists available at SciVerse ScienceDirect

Earth and Planetary Science Letters

journal homepage: www.elsevier.com/locate/epsl

Co-registration of lunar topographic models derived from Chang'E-1, SELENE, and LRO laser altimeter data based on a novel surface matching method

Bo Wu [a,*], Jian Guo [a], Han Hu [a,b], Zhilin Li [a], Yongqi Chen [a]

[a] Department of Land Surveying and Geo-Informatics, The Hong Kong Polytechnic University, Hung Hom, Kowloon, Hong Kong
[b] State Key Laboratory of Information Engineering in Surveying, Mapping and Remote Sensing, Wuhan University, PR China

ARTICLE INFO

Article history:
Received 8 September 2012
Received in revised form
17 December 2012
Accepted 17 December 2012
Editor: T. Spohn

Keywords:
lunar topography
co-registration
surface matching
Chang'E-1
SELENE
LRO

ABSTRACT

Various lunar digital topographic models (DTMs) have been generated from the data collected from earlier and recent lunar missions. There are usually inconsistencies among them due to differences in sensor configurations, data acquisition periods, and production techniques. To obtain maximum value for science and exploration, the multi-source lunar topographic datasets must be co-registered in a common reference frame. Only such an effort will ensure the proper calibration, registration, and analysis of the datasets, which in turn will permit the full comparative and synergistic use of them. This study presents a multi-feature-based surface matching method for the co-registration of multiple lunar DTMs that incorporates feature points, lines, and surface patches in surface matching to guarantee robust surface correspondence. A combined adjustment model is developed for the determination of seven transformation parameters (one scale factor, three rotations, and three translations), from which the multiple DTMs could be co-registered. The lunar DTMs derived from the Chang'E-1, SELENE, and LRO laser altimeter data in the Apollo 15 landing area and the Sinus Iridum area are examined in this study. Small offsets were found among the Chang'E-1, SELENE, and LRO DTMs. Through experimental analysis, the developed multi-feature-based method was proven able to effectively co-register multiple lunar DTMs. The performances of the multi-feature-based surface matching method were compared with the point-based method, and the former was proven to be superior to the latter.

1. Introduction

Lunar topographic information is essential for lunar scientific investigations and lunar exploration missions. For example, high-resolution topographic data are critical for understanding the ring structures, mare fill, ejecta, and other crustal features of impact basins. They have major implications for determining the origin and evolution of the Moon. The Moon's crustal features have largely been established from a combination of satellite-altimetry-derived topography analyses and satellite observations of the lunar gravity field (Potts and von Frese, 2005). The topographic information of lunar impact craters can provide fundamental insights into lunar crust properties, the role of volatiles, and the relative surface age and physics of the craters (Garvin et al., 1999), and their morphological characterizations are significant sources for scientific research. Surface slope measurements are reliable indicators of the importance of gravity-driven processes to a surface. Lunar topographic data also play a critical role in landing-site selection, precision landing, and ground science experiments in lander, vehicle/robot, astronaut, and outpost explorations.

Starting in the 1960s, various lunar topographic products have been created in the Apollo missions (Livingston, 1980; Mellberg, 1997) and the Clementine mission (Smith et al., 1997; Rosiek et al., 1999) to fulfill geoscientist demand. Over the past several years, recent lunar exploration missions, such as the Chinese Chang'E-1 (Ouyang et al., 2010), the Japanese SELenological and ENgineering Explorer (SELENE)/Kaguya (Kato et al., 2008), and NASA's Lunar Reconnaissance Orbiter (LRO) (Chin et al., 2007) have collected a vast amount of lunar topographic data. Laser altimeters and cameras onboard the Chang'E-1, SELENE, and LRO are the primary sensors for collecting lunar topographic information. They have different configurations providing elevation measurements with different characteristics. Various lunar digital topographic models (DTMs) have been generated using the data from the Chang'E-1 Laser AltiMeter (LAM) (Li et al., 2010), SELENE Laser ALTimeter (LALT) (Araki et al., 2009; Noda et al., 2009), and LRO's Lunar Orbiter Laser Altimeter (LOLA) (Smith et al., 2010; Mazarico et al., 2011). They provide great value to scientists who need DTMs for various lunar scientific investigations and explorations. However, among these lunar DTMs derived from different mission data, there are usually inconsistencies, such as translational

* Corresponding author. Tel.: +852 2766 4335; fax: +852 2330 2994.
E-mail address: bo.wu@polyu.edu.hk (B. Wu).

0012-821X/$ - see front matter © 2012 Elsevier B.V. All rights reserved.
http://dx.doi.org/10.1016/j.epsl.2012.12.024

shifts, angular rotations, or scale variations due to differences in sensor configurations, data acquisition periods, and production techniques. For example, Wu et al. (2011) found that there are small shifts (about 350 m and 1.5 km in horizontal and 150 m and 90 m in altitude at the Apollo 15 and 16 landing areas, respectively) between the DTMs derived from the Chang'E-1 LAM and SELENE LALT data. To obtain maximum value for science and exploration, the multi-resolution and multi-scale DTMs derived from different sensors must be co-registered in a common reference frame (Kirk et al., 2012). Only such an effort will ensure (1) the study of offsets, trends, and error analysis in various lunar topographic datasets, (2) the proper calibration and registration of the datasets, (3) the full comparative and synergistic use of the datasets, and (4) the generation of consistent and precise lunar topographic products.

Multiple lunar topographic datasets can be categorized into two co-registration types, including strategic and tactical co-registrations. Strategic co-registration must be performed globally and in a way that addresses internal errors and variations in the datasets. An *a priori* uncertainty analysis of each dataset is necessary to produce a combination with the highest possible accuracy. Tactical co-registration is related to the alignment of regional lunar topographic datasets from different sources. Over a relatively small regional area, any differences in coordinate definitions and the systematic varying errors of calibration are expected to appear as offsets and rotations and could be reduced by transforming the entire dataset.

This study focuses on the tactical co-registration of multiple lunar DTMs through a novel surface matching method to reduce the inconsistencies between them and, subsequently, to produce precise lunar topographic models. After presenting a literature review on lunar topographic products from various lunar missions and state-of-the-art co-registration methods between multiple datasets, an innovative surface matching method that incorporates feature points, lines, and surface patches interactively derived from the lunar topographic models is presented in detail. The DTMs derived from the Chang'E-1 LAM, SELENE LALT, and LRO LOLA data at two experimental sites (the Apollo 15 landing area and the Sinus Iridum area) are examined and analyzed. The performances of the proposed surface matching method are evaluated. Finally, concluding remarks are presented and discussed.

2. Related work

2.1. Lunar topographic models from earlier and recent missions

From earlier and recent lunar exploration missions, a vast amount of lunar topographic data has been produced using lunar surface images and elevation measurements collected by the cameras and laser altimeters onboard the spacecraft. In the Apollo era, a variety of photographic sources and laser altimeter measurements collected during the Apollo program were used for lunar topographic modeling. Lunar topographic maps at scales of 1:1,000,000 and 1:250,000 have been produced using metric camera photographs from the Apollo 15, 16, and 17 missions (Livingston, 1980; Mellberg, 1997). The laser altimeter attached to the metric camera systems onboard these three Apollo missions had a ground footprint of about 20 m and the laser altimeter data were used to constrain the bundle adjustment of the mapping camera data. The Clementine mission in 1994 provided the first near-global mapping of the Moon. The laser altimeter onboard the Clementine spacecraft collected elevation measurements of the lunar surface and the data were used to generate a topographic model of the Moon. The model had an absolute vertical accuracy of approximately 100 m and a spatial resolution of 2.5° (Smith et al., 1997). The United States Geological Survey (USGS) also generated a global digital image model (100 m/pixel) of the Moon using the images collected by the onboard ultraviolet–visible camera (Eliason et al., 1999). In 2006, USGS released a Unified Lunar Control Network (ULCN) 2005 consisting of the 3D position of 272,931 points, which is based on a photogrammetric solution of 43,866 Clementine images and earlier data (Archinal et al., 2006).

In October 2007, China launched Chang'E-1, its first lunar probe (Ouyang et al., 2010). The LAM onboard the Chang'E-1 spacecraft collected more than 9 million range measurements covering the entire Moon, of which about 3.2 million were useful for topographic modeling (Li et al., 2010). The Chang'E-1 LAM data had spacing resolutions of 1.4 km for the along-track direction and 7 km for the cross-track direction (at the equator). A global lunar digital elevation model (DEM) with a 3-km spatial resolution was produced using the LAM data. The plane positioning accuracy of the DEM was 445 m, and the vertical accuracy was 60 m (Li et al., 2010). The CCD camera onboard the Chang'E-1 spacecraft returned 1098 orbiter images with a spatial resolution of 120 m. A global DEM with 500 m grid spacing was also produced using these images (Liu et al., 2009). Regional DEMs with 360-m grid spacing were generated at the Apollo 15 and 16 landing areas by integrating the Chang'E-1 LAM and image data (Wu et al., 2011). The Chang'E-1 data are currently publically available in Planetary Data System (PDS) format through the Lunar Exploration Data Release System (http://159.226.88.59:7779/CE1OutENGWeb/step.jsp). China's second lunar probe, Chang'E-2, was launched in October 2010. Chang'E-2 carried a similar suite of instruments to Chang'E-1, but the laser altimeter and CCD camera were both improved. The Chang'E-2 imagery had global 7 m/pixel coverage and regional coverage of Sinus Iridium at 1.5 m/pixel. Regional lunar topographic models were produced using the Chang'E-2 data (Di et al., 2012; Zou et al., 2012).

The Japanese lunar explorer SELENE was launched in September 2007 (Noda et al., 2009). Its onboard LALT collected more than 20 million range measurements, of which 10 million had high-quality orbital data and were used for topographic modeling (Araki et al., 2009). The SELENE LALT data covered the entire region of the Moon with a height resolution of 5 m at a sampling interval smaller than 2 km. A global lunar topographic map with a spatial resolution of 0.5° was derived from the SELENE LALT data (Araki et al., 2009). SELENE also acquired stereoscopic images with 10-m resolution using its push-broom Terrain Camera, which covered almost the entire surface of the Moon. A global DTM mosaic with 10-m spatial resolution was produced from the camera imagery (Haruyama et al., 2012). The SELENE data are publically available in the SELENE Data Archive (http://l2db.selene.darts.isas.jaxa.jp/index.html.en).

NASA successfully launched its LRO to the Moon in June 2009. The LOLA onboard the LRO is a pulse detection altimeter that incorporates a five-spot X-pattern, measuring the distance to the lunar surface at five spots simultaneously (Smith et al., 2010). LOLA has so far collected more than 5.5 billion valid range measurements (Kirk et al., 2012). The five-spot pattern provides five adjacent profiles for each track, 10–12 m apart over a 50- to 60-m swath, with combined measurements in the along-track direction every 10–12 m. The across-track resolution depends on the spacecraft's number of orbits, and after one year of operation is approximately 0.04° (about 1.2 km at the equator) (Smith et al., 2010). A topographic map of the near side of the Moon has been generated using 1 billion LOLA measurements at a spatial resolution of 20 m along track and a 0.1° ground-track spacing (Riris et al., 2010). The wide-angle cameras (WACs) and narrow-angle cameras (NACs) onboard LRO have collected lunar images at resolutions of 100 m/pixel and 50 cm/pixel, respectively. The WAC images have proven global coverage, and a near-global DTM GLD100 with a pixel spacing of 100 m has been produced from the WAC images

(Scholten et al., 2012). However, the WAC images in GLD100 are uncontrolled, so there are positional errors of unknown magnitude and these can vary framelet by framelet, and certainly orbit by orbit. NAC images cover only a small portion of the lunar surface, but have included complete coverage of both poles (Robinson et al., 2012; Waller et al., 2012). Regional DTMs with meter-level resolution have been generated from the NAC images (Tran et al., 2010; Li et al., 2010; Burns et al., 2012). The LRO data are publically available through the PDS Geosciences Node (http://pds-geosciences.wustl.edu/missions/lro/) and PDS Imaging Node (http://pds-imaging.jpl.nasa.gov/volumes/lro.html).

2.2. Co-registration of multiple topographic models

For surface comparison or co-registration between different topographic models, vast efforts have been exerted on Earth topographic datasets in the past. Williams et al. (1999) studied the registration of three-dimensional datasets with rigid motions. The registration process comprises two steps: correspondence selection and motion estimation. Besl and McKay (1992) presented an iterative closest point (ICP) algorithm for surface matching. The key function of the ICP algorithm is to search for pairs of the closest points in the two datasets, estimating the rigid transformation and iteratively refining the transformation by repeatedly generating pairs of closest points on the two sets by minimizing an error metric. However, the ICP algorithm has several drawbacks: (1) it is time consuming due to the exhaustive search for the closest points; (2) good initial approximations of the closest points are required for the convergence of the iteration calculations; (3) the closest point pairs are sometimes unreliable, especially for topographic models with low spatial resolutions; and (4) possible errors in point selection will lead to unfavorable surface matching results. Li et al. (2001) presented a surface matching technique to detect the local deformation of a surface using a least-median-of-squares estimator. Gruen and Akca (2005) described a least squares 3D surface matching method. This method is able to estimate the 3D transformation parameters between two or more surface patches using the generalized Gauss–Markov model by minimizing the sum of the Euclidean distance squares between the surfaces. However, good initial approximations of the transformation parameters are required in their method. Streutker et al. (2011) presented a slope-based method for the co-registration of overlapping elevation surfaces. This method is used to realign the flight lines of light detection and ranging (LiDAR) datasets, and results show that the decimeter offsets between different LiDAR flight lines can be reduced. However, this method may perform poorly if the initial offsets between the two surfaces are relatively large.

Few studies have emphasized the co-registration of multiple lunar topographic models. Rosiek et al. (2001) described a method to co-register the Clementine images with the Clementine laser altimeter data, in which the Clementine global mosaic was used to establish horizontal control and Clementine laser altimeter points were used for vertical control. However, due to the marginal overlap between stereo models, the geometry of the photogrammetric network was weak and resulted in stereo models that did not align with each other. Di et al. (2010) presented a co-registration method of lunar DTMs derived from the Chang'E-1 stereo images and the laser altimeter data to reduce the inconsistencies between them. In their method, a DTM is generated first from the stereo images, and then the DTM is registered to the LAM data through surface matching using an ICP algorithm (Besl and McKay, 1992). Through surface matching, a 3D rigid transformation model (with three rotation and three translation parameters) between the DTMs can be obtained, from which the exterior orientation (EO) parameters of the images are adjusted so that the images and laser altimeter data are co-registered. Di et al. (2012) further examined the crossover adjustment of the Chang'E-1 laser altimeter data, and then used the ICP algorithm to co-register the Chang'E-1 stereo images with the refined laser altimeter data. Wu et al. (2011) developed a bundle adjustment approach to integrate the Chang'E-1 imagery and laser altimeter data for precision lunar topographic modeling. The bundle adjustment model involves the laser altimeter points, image EO parameters, and tie points collected from the stereo images. The output of the adjustment is the refined image EO parameters and laser ground points. After the bundle adjustment process, the misregistrations between the Chang'E-1 imagery and the laser altimeter data are reduced from as large as 18 pixels to about 1 pixel in image space. Guo and Wu (2012) examined the co-registration between the DTMs derived from the Chang'E-1 and SELENE laser altimeter data using a least squares surface matching method based on tie points identified from the DTMs. Seven transformation parameters (one scale factor, three rotations, and three translations) are employed in this co-registration method. Results show that small shifts between these two datasets are reduced after co-registration. Beyer et al. (2010, 2011) and Rosiek et al. (2012) presented some initial results of comparison of LRO NAC DTMs.

Co-registration of multiple topographic models has been examined for Mars topographic datasets. Anderson and Parker (2002) examined the precision registration between Mars orbiter camera (MOC) imagery and Mars orbiter laser altimeter (MOLA) data at selected candidate landing sites. Yoon and Shan (2005) presented a combined adjustment method to process the MOC imagery and MOLA data and indicated that the large misregistration between the two datasets could be corrected to a certain extent. Spiegel (2007) developed a high-resolution stereo camera (HRSC) imagery bundle adjustment technique, in which a sparse stereo point cloud is adjusted to optimize its fit to a surface interpolated from the MOLA data. This adjustment is now standard in the production of controlled orthorectified HRSC products. Lin et al. (2010) developed a co-registration process to align Mars DTMs derived from the MOLA, HRSC, and high-resolution imaging science experiment (HiRISE). The base algorithm for co-registration is a 3D conformal co-ordinate transformation including seven parameters (three translations, three rotations, and one scale factor). Instead of simply taking the closest point pairs on the DTMs for the transformation parameter solution, an enclosing surface patch is used for better approximation of corresponding points. Delaunay triangulations of the DTMs are constructed. They are used to find the enclosing triangles of point pairs in the triangulations, which enables a better height value to be interpolated than if only the single closest point is used. Lin et al. (2010) also presented an assessment of surface matching parameters for the co-registration of multi-resolution Mars DTMs.

Based on previous studies, this study presents a novel surface matching method for the co-registration of multiple lunar topographic models. This method incorporates feature points, lines, and surface patches into the surface matching to guarantee robust surface correspondence, which is hard to achieve from the traditional point-based surface matching method. Strict mathematic models of using feature lines and surface patches for surface matching have been developed, which to our knowledge are new in the field of surface matching. It should be noted that while the focus of this study is the co-registration of lunar DTMs derived from the Chang'E-1 LAM, SELENE LALT, and LRO LOLA laser altimeter data, the developed method can also be used for the co-registration of lunar DTMs derived from various sources, e.g., lunar laser altimeter data and lunar orbiter images.

3. A novel surface matching method based on multiple features

3.1. Overview of the approach

For two lunar DTMs derived from different sources of laser altimeter data, one is treated as a reference DTM (e.g., DTM 1) and the other as a matching DTM (e.g., DTM 2). Feature points, lines, and surface patches are identified on both DTMs for surface matching. The feature points are normally the centers of craters or other terrain feature points. The feature lines are the ridge or valley lines detected from the DTMs. To obtain feature surface patches, the DTMs are segmented through triangulations, and the triangles that share surface normals are merged to form local surface patches. The feature points, lines, and surface patches are then used as inputs in the combined adjustment model. The outputs comprise seven transformation parameters (one scale factor, three rotations, and three translations), from which the matching DTM can be co-registered to the referencing DTM. Fig. 1 shows the overview of the approach.

It should be noted that if the spatial resolutions of the two DTMs are different, then the DTM with a higher resolution will be resampled to a new DTM with the same resolution. Surface matching is carried out between the two equal-resolution DTMs, while the obtained transformation parameters are applied to the original DTMs for further co-registration and analysis.

3.2. Combined adjustment model

For the co-registration of multiple DTMs using point pairs, the relationship between a point $P(X_P,Y_P,Z_P)^T$ on the reference DTM and a point $P'(X_{P'},Y_{P'},Z_{P'})^T$ on the matching DTM can be represented using the following equation (Mills et al., 2003):

$$P = sRP' + T \tag{1}$$

where s is a scale factor denoting the magnification or contraction between the two DTMs, R is a rotation matrix that is determined entirely by three Euler rotation angles (φ,ω,κ), and $T=(T_X,T_Y,T_Z)^T$ is a 3D translation vector between the two DTMs. In Eq. (1), the seven parameters s, (φ,ω,κ) and (T_X,T_Y,T_Z) are all unknowns that need to be solved. Each point pair generates three observation equations.

The following describes the mathematical model of using line pairs for surface matching. As shown in Fig. 2, a line pair (L, L') is identified on the two DTMs. P_1 and P_2 are on line L on the reference DTM and P_3' and P_4' are on line L' on the matching DTM. If the seven transformation parameters are perfectly accurate, the corresponding points of P_3' and P_4', which are P_3 and P_4, should be collinear with points P_1 and P_2. Therefore, the distance from point P_3 (or P_4) to line L should be 0 in the ideal situation. A mathematical model that uses line pairs for surface matching is built based on this observation.

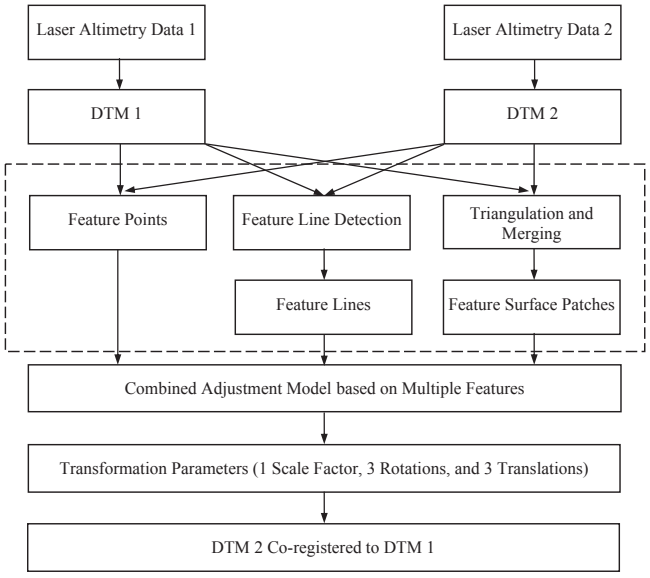

Fig. 1. Framework of the surface matching method.

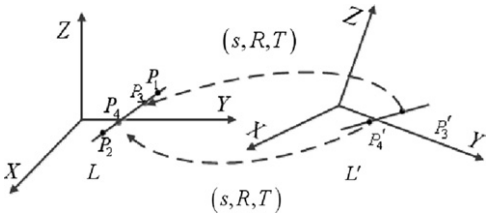

Fig. 2. Illustration for line co-registration.

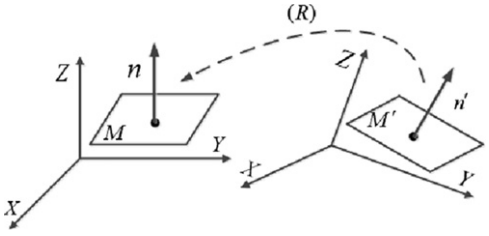

Fig. 3. Illustration for surface patch co-registration.

Assuming a 3D line L is determined by points P_1 and P_2, it can be mathematically modeled by the intersection of two space planes as shown in the following equation:

$$L\begin{cases} m_{11}x+m_{12}y+m_{13}z=b_1 \\ m_{21}x+m_{22}y+m_{23}z=b_2 \end{cases} \tag{2}$$

Eq. (2) can be expressed in matrix form as

$$MX = B \tag{3}$$

where

$$M=\begin{pmatrix} m_{11} & m_{12} & m_{13} \\ m_{21} & m_{22} & m_{23} \end{pmatrix},\quad B=\begin{pmatrix} b_1 \\ b_2 \end{pmatrix},\quad X=\begin{pmatrix} x & y & z \end{pmatrix}^T,$$

forming the line equation.

For a point P' (e.g., P_3' or P_4') on line L', the distance from its corresponding point P (P_3 or P_4) to line L can be determined by the following equation:

$$d = \sqrt{(B-MP)^T(MM^T)^{-1}(B-MP)} \tag{4}$$

In the ideal situation, the distance d should be 0. The constraint $d=0$ is then used for line correspondence in the adjustment model. The matrices B and M in Eq. (4) are related to line L and determined by points P_1 and P_2. P (e.g., P_3 or P_4) in Eq. (4) is determined by point P' (P_3' or P_4') through Eq. (1). For each line correspondence, two distance constraints can be generated independently, as two points are determinants for a line. Therefore, each line correspondence will produce two observation equations.

From the preceding discussion, it can be seen that there is no point correspondence (e.g., correspondence of line end points) requirement in the line-matching model. Two corresponding lines, each determined by any two points, can be used for line matching, even though the lengths of the two lines could vary. This line-matching strategy provides more robust correspondence compared with point pairs.

For the correspondence between two surface patches, the normal vectors of the surface patches are used for surface matching. As

shown in Fig. 3, the relationship between a surface patch M and its corresponding surface patch M' can be determined by their surface normals $n(n_X, n_Y, n_Z)^T$ and $n'(n_{X'}, n_{Y'}, n_{Z'})^T$ through the following equation:

$$n = Rn', \tag{5}$$

where R is the rotation matrix determined by the rotation angles (φ,ω,κ), as described previously in Eq. (1). For each corresponding surface (normal vector), three observation equations can be generated that are related only to the rotation matrix.

After linearizing Eqs. (1), (4) and (5) with respect to the seven unknown transformation parameters, the observation equations for the combined adjustment can be represented in matrix form as

$$V = AX - L, P \tag{6}$$

where X is the unknown vector to be solved containing the transformation parameters (s, R, T), L is the observation vector, A is the coefficient matrix containing the partial derivatives from each observation, and P is the *a priori* weight matrix of the observations that reflects the measurement quality and the contribution of the observation to the final result. In particular, the combined adjustment in this method includes the following three parts for the three different types of observations:

$$\begin{aligned} V_1 &= A_1X_1 + B_1X_2 + C_1X_3 - L_1, P_1 \\ V_2 &= B_2X_2 - L_2, P_2 \\ V_3 &= A_3X_1 + B_3X_2 + C_3X_3 - L_3, P_3 \end{aligned} \tag{7}$$

The first equation in Eq. (7) is the observation equation for the point correspondence, in which X_1 is the unknown scale parameter, X_2 represents the vector of unknown rotation angles (φ,ω,κ), and X_3 is the vector of unknown translation parameters. The coefficient matrix A in Eq. (6) is divided into A_i, B_i, and C_i $(i=1–3)$ for different types of unknown parameters. The second equation represents the observation residuals of normal vectors of the corresponding surface patches. As denoted in this equation, the surface normal is only related with the unknown rotation angles. The third equation is the observation equation for line correspondence after applying the distance constraint $d=0$. For different types of observation equations, different weights P_i $(i=1–3)$ are assigned (details discussed in Section 3.4).

Since this study focuses on co-registration of multiple lunar topographic models in local regions, the geometric centroid of the study area is used as the rotation origin. The seven unknown transformation parameters are calculated through a least squares minimization of difference between the matching surface and the reference surface based on Eq. (7). It should be noted that this adjustment model has the flexibility to use individual types of feature points, lines, and surface patches or any combination of the three for surface matching, depending on the types of features that can be detected from the DTMs. If only the surface patches are used, only the three rotation angles can be determined. Feature lines or points are necessary to determine the translation parameters and the scale factor.

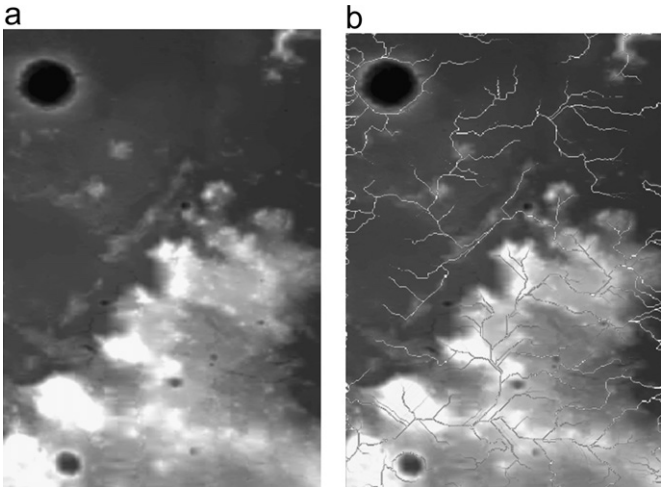

Fig. 4. Feature line extraction. (a) A DTM derived from the LRO LOLA data in the Apollo 15 landing area and (b) the extracted feature lines on the DTM.

3.3. Determination of multiple features

3.3.1. Feature point determination

Co-registration of multiple DTMs from feature points is the most common and easiest method. Popular approaches are largely based on the ICP algorithm (Besl and McKay, 1992). However, as discussed previously, the ICP algorithm has several drawbacks, and even the closest points derived through the iterative calculations in the ICP algorithm do not necessarily have to be the exact corresponding points on both DTMs. This is especially true for lunar DTMs derived from different sources; they usually have low spatial resolutions of several hundred meters or kilometers, and there are usually

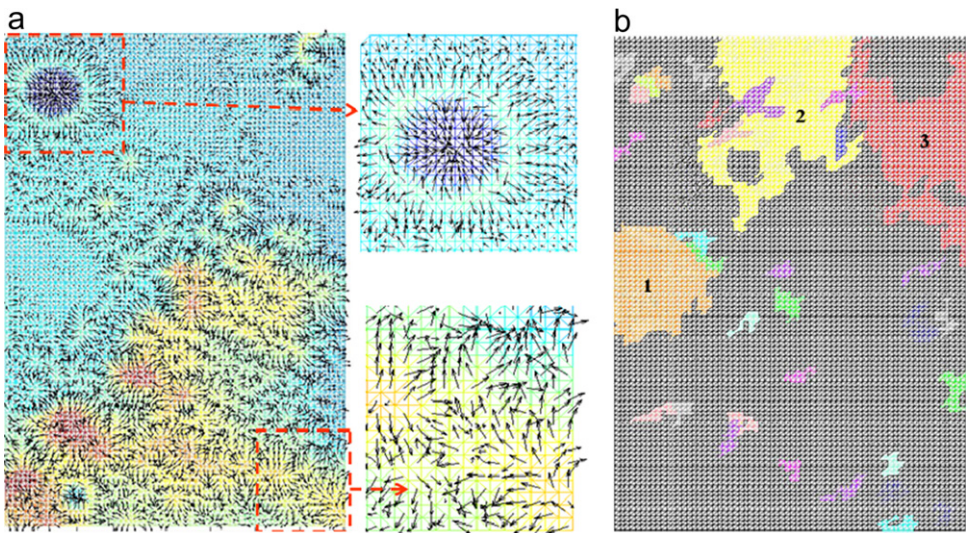

Fig. 5. Feature surface patch extraction. (a) Triangulation of the DTM and surface normal within each triangle and (b) the extracted feature surface patches on the DTM. (For interpretation of the references to color in this figure legend, the reader is referred to the web version of this article.)

inconsistencies between them. A tiny discrepancy in the point pairs will lead to large variations in the transformation parameters.

Only feature points that can be clearly identified on the DTMs, such as the centers of craters or other terrain feature points, are used in the adjustment model. 2D DTM gray-scale maps (e.g., Fig. 4(a)) are used to determine the crater centers. The circles or ellipses that best fit the boundaries of the craters in the 2D gray-scale maps are determined, and the centers of the circles or ellipses are selected as the planar locations of the crater centers. The altitudes of the crater centers are derived from the DTMs based on their planar locations. To determine the terrain feature points, skeleton lines (ridge or valley lines) are first extracted on the DTMs based on a terrain analysis algorithm (Tarboton, 1997), and the intersection points of the skeleton lines with similar patterns in the local regions (e.g., point 3 in Fig. 7(a) and (b)) are selected as the terrain feature points. Their 3D coordinates can be derived from the DTMs. The matches of these feature points are performed interactively. These feature points have low priority in the adjustment model compared with feature lines and surface patches due to the possible uncertainties in determining them. As such, fewer feature points are used and they are assigned smaller weights in the adjustment model.

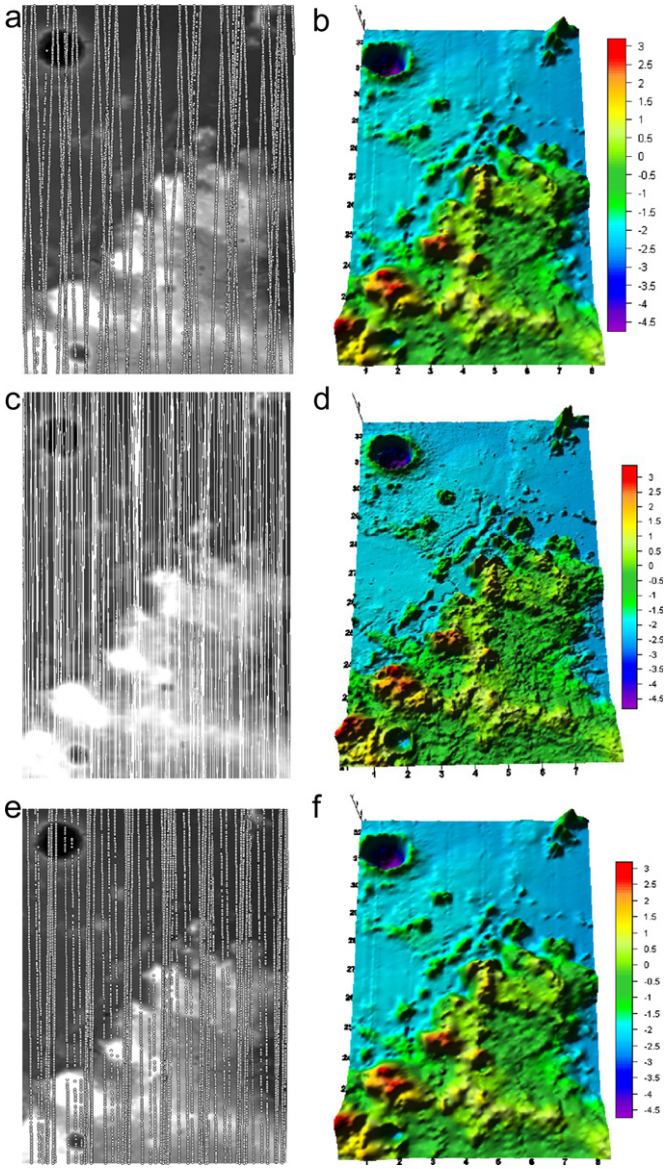

Fig. 6. Chang'E-1 LAM, LRO LOLA, and SELENE LALT data and DTMs in the Apollo 15 landing area. (a) Chang'E-1 LAM data (9863 points) overlaid on the DTM, (b) 3D view of the Chang'E-1 DTM, (c) LRO LOLA data (1,132,676 points) overlaid on the DTM, (d) 3D view of the LRO DTM, (e) SELENE LALT data (11,595 points) and (f) 3D view of the SELENE DTM.

3.3.2. *Feature line determination*

The feature lines are the important skeleton lines (ridge or valley lines) on the DTM. As mentioned above, a terrain analysis algorithm (Tarboton, 1997) was used in this study to extract feature lines from multiple lunar DTMs. Fig. 4 shows an example of the feature line extraction. Fig. 4(a) is a DTM interpolated from the LRO LOLA data in the Apollo 15 landing area, in which light colors represent higher elevation areas and darker colors represent lower elevation areas. Fig. 4(b) shows the results of feature line extraction. It is apparent that a large number of feature lines can be successfully extracted from the DTM. After the feature lines were extracted from multiple DTMs, those common line segments that could be clearly identified were used in the adjustment model to determine the transformation parameters.

As discussed previously, surface matching based on feature lines is more robust than the point-based method. Feature lines are particularly useful in determining the translation parameters between the multiple DTMs. In theory, two pairs of feature lines are enough to determine the three translation parameters. More feature lines can be used to refine the results through a least squares adjustment. Because feature lines may have relatively

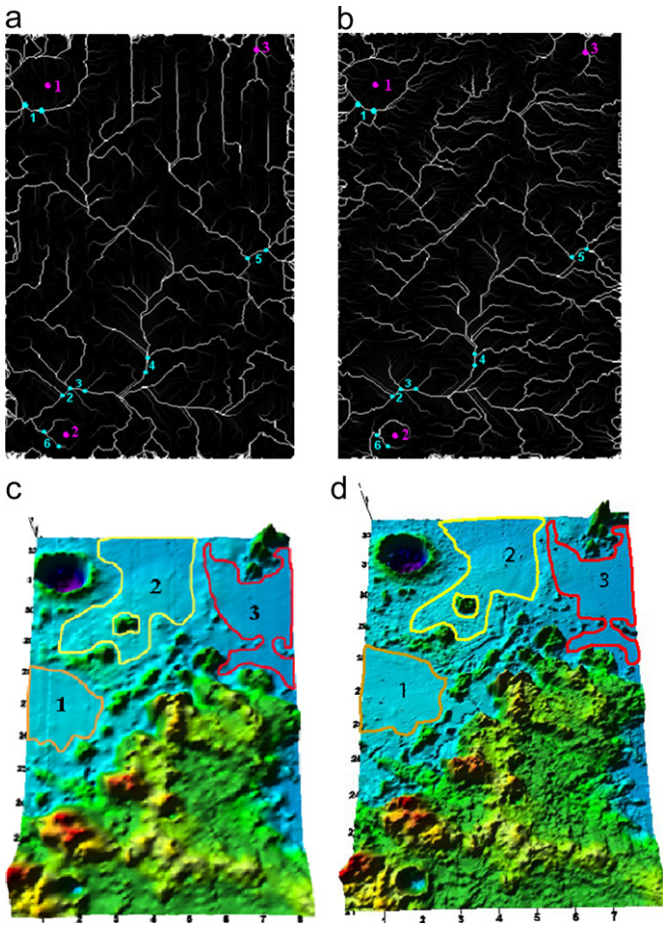

Fig. 7. Feature points, lines, and surface patches determined on the Chang'E-1 and LRO DTMs in the Apollo 15 landing area. (a) The selected feature points (marked with purple) and line segments (cyan) on the Chang'E-1 DTM, (b) the corresponding feature points and line segments on the LRO DTM, (c) the selected surface patches on the Chang'E-1 DTM and (d) the corresponding surface patches on the LRO DTM. (For interpretation of the references to color in this figure legend, the reader is referred to the web version of this article.)

Table 1
Transformation parameters between the Chang'E-1 and LRO DTMs in the Apollo 15 landing area.

Transformation parameters	Multi-feature-based method	Point-based method
Scale	0.9978	0.9986
ΔX (longitude)	−1.92 m	110.77 m
ΔY (latitude)	24.44 m	43.39 m
ΔZ (altitude)	−217.63 m	−883.15 m
$\Delta\varphi$ (roll)	0.014°	0.036°
$\Delta\omega$ (pitch)	0.011°	−0.0005°
$\Delta\kappa$ (yaw)	−0.001°	0.0043°

weak control in determining the rotation angles between the multiple DTMs, surface patches are employed in this approach to determine rotation transformation parameters. This is described in the following subsection.

3.3.3. Feature surface patch determination

Feature surface patches are normally planar sub-surface patches on the DTM. Corresponding surface patches on multiple DTMs can provide robust rotation transformations between the DTMs. To obtain feature surface patches on the DTM, first, a triangulation of the DTM is performed by dividing each grid in the DTM into two triangles. Next, a surface normal is calculated for each triangle, which is a vector originating at the triangle center that points to the outer side and is perpendicular to the triangle plane. Starting from any triangle in the triangulation, a merging process is performed to merge its neighbor triangles into a surface patch by comparing the differences between their surface normals with a predefined threshold. The threshold is determined by considering the cosine value of the angle between the two adjacent surface normals. If the value is close to 1, the angle between the two surface normals is small enough, and the two triangles can be considered to share the same surface location. A threshold of 0.985 (about 10°) was used for all of the DTMs in this study's experiments. This merging process is continued until all of the triangles in the triangulation are examined. To ignore the small-scattered surface patches, only surface patches whose number of merged triangles meet a threshold are finally selected. Fig. 5 shows an example of feature surface patch extraction.

Fig. 5(a) is the triangulation of the DTM shown in Fig. 4(a). In Fig. 5(a), brown and yellow areas represent higher elevation areas, and cyan and blue areas represent lower elevation areas. The surface normals of each triangle are represented with black arrows, as can be seen in the enlarged figures. The final identified surface patches are represented with different colors in Fig. 5(b). The areas not belonging to surface patches are indicated with black. After surface patches on the DTMs are selected, the average surface normal of the triangles within each surface patch are calculated and used as the surface normal for the surface patch. It is notable that only surface patches that can be clearly identified on both the DTMs are used in the adjustment model. They are usually relatively large surface patches, such as those marked with 1, 2, and 3 in Fig. 5(b).

It should be noted that we developed automatic software programs to extract feature points, lines, and surface patches from the DTMs. The matching of these features in multiple DTMs must be performed interactively at this stage.

3.4. Weight determination in the adjustment model

The adjustment model employs pseudo-observation equations constructed from the participants (feature points, lines, and surface patches). Though this is a useful and common treatment in adjustment methodology because it provides the flexibility to properly weight the participants in the adjustment (Mikhail et al., 2001), it also introduces difficulties in how to assign appropriate weights to the adjustment model participants. The weights are determined by both the different magnitudes of order across different units and the *a priori* measured accuracies of the participants. In general, the more accurate and reliable participants will have higher weights in the adjustment.

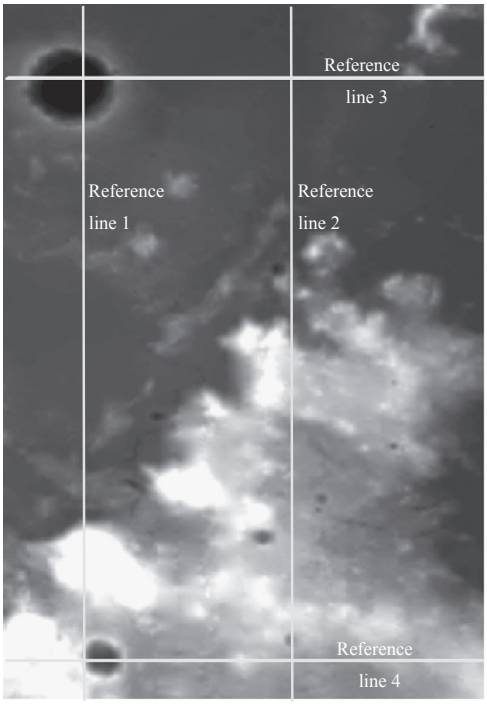

Fig. 8. Four reference lines selected for comparison analysis in the Apollo 15 landing area.

For the three types of participants (feature points, lines, and surface patches) used in this approach, the feature surface patches are determined through the cluster of triangulations based on the local-area terrain trends, which contribute to the calculation of the three rotation parameters in the surface matching. The feature lines are identified according to similar feature terrain line segments, providing robust determination of the three translation parameters and also contributing to the calculation of other transformation parameters. The feature lines and surface patches are considered the most accurate measurements in the adjustment model. Therefore, a unit weight is assigned to all of the surface normals and feature lines. The feature points are identified mostly at the centers of craters or other terrain feature points, which are considered to be the relatively less reliable measurements in the adjustment model. In addition, the point correspondences are more sensitive to noises in the DTM. These noises cause disturbances around the points that can be eliminated in the line detection and surface growing process. The feature points are assigned a weight much smaller than the unit weight based on their *a priori* variance. It is apparent from previous experience in photogrammetry (Yoon and Shan, 2005) that the adjustment model is less sensitive to weight assignments. Moderate changes in weight magnitude yield similar results.

4. Co-registration of multiple lunar DTMs derived from Chang'E-1 LAM, SELENE LALT, and LRO LOLA data

The developed multi-feature-based surface matching method was used to co-register the multiple DTMs derived from the Chang'E-1 LAM, SELENE LALT, and LRO LOLA data in the Apollo 15 landing area and the Sinus Iridum area. The details are described in the following subsections.

4.1. Co-registration of multiple lunar DTMs in the Apollo 15 landing area

The Apollo 15 landing site is located at (3.66°E, 26.08°N) at the foot of the Apennine Mountain range. The experimental area in this study covered a region of 0.5–8°E and 21–32°N, including diverse terrain features such as the Apennine Mountain, Autolycus Crater, and Hadley Rille. The maximum elevation difference is about 8 km, from the peak of the Apennine Mountain to the bottom of the Autolycus Crater. Fig. 6 shows the distributions of

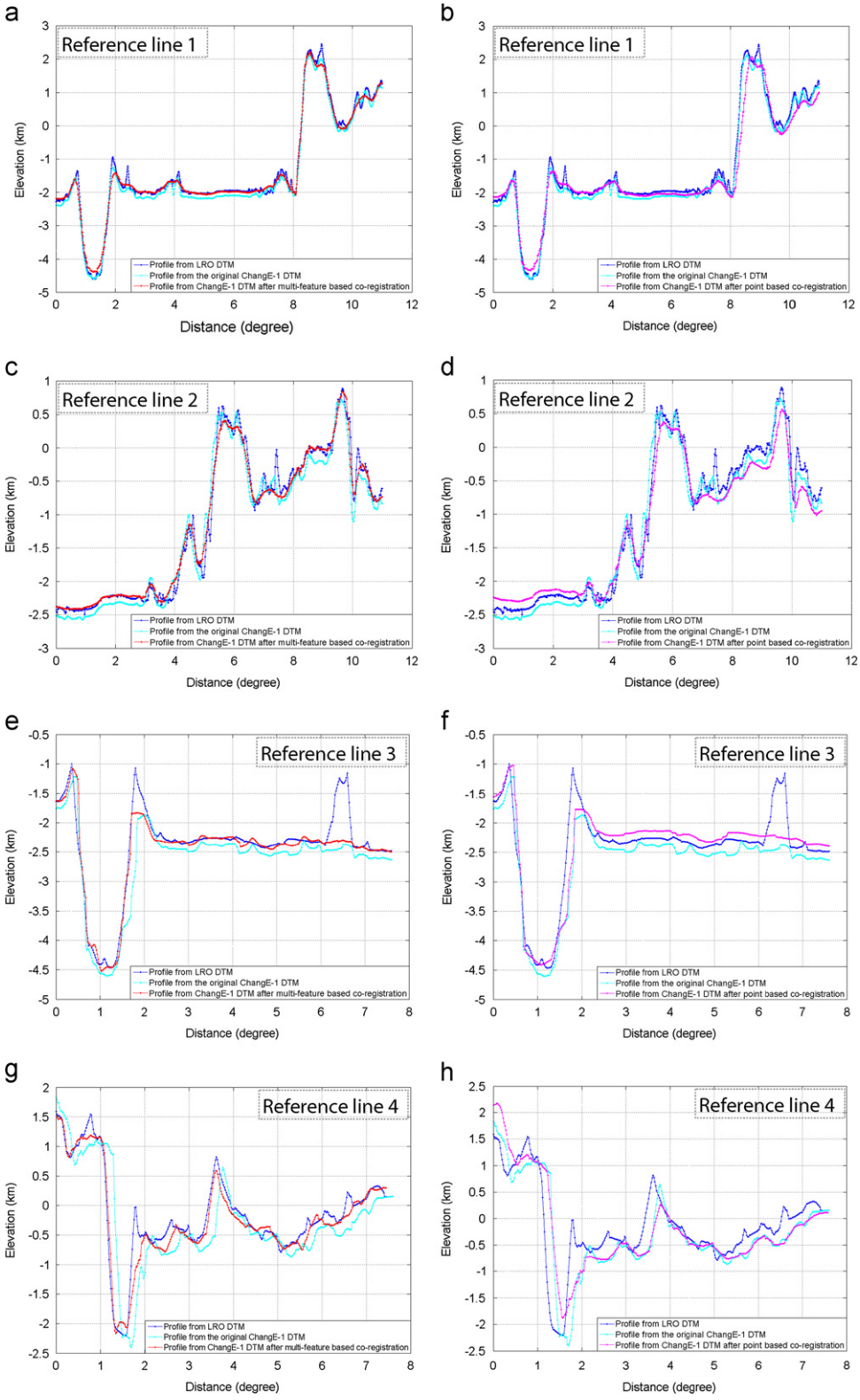

Fig. 9. Profiles derived from the LRO and Chang'E-1 DTMs in the Apollo 15 landing area. (a) Profiles for reference line 1 using multi-feature based co-registration, (b) profiles for line 1 using point based co-registration, (c) profiles for line 2 using multi-feature based co-registration, (d) profiles for line 2 using point based co-registration, (e) profiles for line 3 using multi-feature based co-registration, (f) profiles for line 3 using point based co-registration, (g) profiles for line 4 using multi-feature based co-registration and (h) profiles for line 4 using point based co-registration. (For interpretation of the references to color in this figure, the reader is referred to the web version of this article.)

Table 2
Statistics of the absolute elevation differences between the profiles derived from the Chang'E-1 and LRO DTMs in the Apollo 15 landing area.

	Average	Maximum	Minimum	Standard deviation
	(m)	(m)	(m)	(m)
Reference line 1				
LRO profile–Chang'E-1 profile (original)	97.48	838.38	3.41	261.86
LRO profile–Chang'E-1 profile (multi-feature-based method)	9.27	792.40	0.25	189.75
LRO profile–Chang'E-1 profile (point-based method)	71.50	1601.81	0.22	168.92
Reference line 2				
LRO profile–Chang'E-1 profile (original)	73.19	958.86	0.11	197.33
LRO profile–Chang'E-1 profile (multi-feature-based method)	8.84	700.15	0.00	188.22
LRO profile–Chang'E-1 profile (point-based method)	63.21	815.94	0.12	130.23
Reference line 3				
LRO profile–Chang'E-1 profile (original)	223.75	1756.30	6.30	338.14
LRO profile–Chang'E-1 profile (multi-feature-based method)	102.04	1724.90	0.10	318.15
LRO profile–Chang'E-1 profile (point-based method)	170.10	1548.60	0.50	331.07
Reference line 4				
LRO profile–Chang'E-1 profile (original)	138.47	2785.30	2.20	536.22
LRO profile–Chang'E-1 profile (multi-feature-based method)	57.24	1063.30	0.30	172.40
LRO profile–Chang'E-1 profile (point-based method)	75.29	2225.20	0.60	521.60

Table 3
Transformation parameters between the SELENE and LRO DTMs in the Apollo 15 landing area.

Transformation parameters	Multi-feature-based method
Scale	0.9995
ΔX (longitude)	−39.08 m
ΔY (latitude)	9.89 m
ΔZ (altitude)	164 m
$\Delta\varphi$ (roll)	0.0025°
$\Delta\omega$ (pitch)	−0.0121°
$\Delta\kappa$ (yaw)	−0.0002°

the laser altimeter points from Chang'E-1 LAM, LRO LOLA, and SELENE LALT at the study area. There were 9683, 1,132,676, and 11,595 points from Chang'E-1 LAM, LRO LOLA, and SELENE LALT, respectively. DTMs sharing a 0.02° grid spacing resolution (about 600 m in latitude and 400 m in longitude) were interpolated from the laser altimeter points, respectively. The points were overlaid on their corresponding DTMs as illustrated in Fig. 6(a), (c), and (e). Fig. 6(b), (d), and (f) show the 3D view of the DTMs.

4.1.1. Co-registration of Chang'E-1 and LRO DTMs in the Apollo 15 landing area

The developed multi-feature-based surface matching method was used to co-register the Chang'E-1 DTM to the LRO DTM. Feature points, lines, and surface patches were detected from both of the DTMs using the methods described in Section 3.3. Finally, three point pairs (two crater centers and one mountain peak) and six line pairs were identified from the two DTMs as illustrated in Fig. 7(a) and (b). Three pairs of surface patches were also identified from the two DTMs as shown in Fig. 7(c) and (d). They were then used as inputs in the adjustment model for surface matching.

After surface matching using the developed method, seven transformation parameters including one scale factor, three translations, and three rotations were obtained. They are listed in Table 1. The results show that for the DTMs derived from the Chang'E-1 LAM and LRO LOLA data in the Apollo 15 landing area, there are about 25 m offset between these two datasets in the horizontal direction, and the LRO data are about 218 m higher than the Chang'E-1 data. The deviations in rotations between these two datasets are small, and the scales are very similar. Another point-based-surface matching method was also tested. In this method, several point pairs were identified from the DTMs, and a similar strategy with the ICP algorithm was employed to obtain the closest points based on the initial identified point pairs. After that, the closest points were used as inputs in an adjustment model based on Eq. (1). Similarly, the geometric centroid of the study area was used as the rotation origin and seven transformation parameters were finally obtained. Twelve point pairs including the three used in the previous method were used for the Chang'E-1 and LRO DTMs in the Apollo 15 landing area, and the obtained transformation parameters are also listed in Table 1.

The obtained transformation parameters were used to transform the Chang'E-1 LAM point set to a new frame, and a new DTM was interpolated from the new point set. This co-registration process brought the new Chang'E-1 DTM into alignment with the LRO DTM. To evaluate the co-registration method performances, four reference lines were selected for profile comparison analysis as shown in Fig. 8, of which lines 1 and 2 are along the north–south direction and lines 3 and 4 are along the east–west direction.

Three profiles were derived for each reference line, including a profile derived from the LRO DTM, a profile derived from the original Chang'E-1 DTM, and a profile derived from the Chang'E-1 DTM after co-registration. Fig. 9(a), (c), (e) and (g) show the results from the multi-feature-based co-registration, and Fig. 9(b), (d), (f) and (h) show the results from the point-based co-registration.

Fig. 9 shows that the general trends among these profiles are consistent for the four reference lines in this study area. The profiles derived from the Chang'E-1 DTMs show relatively smooth topography compared with the profiles derived from the LRO DTM. This is because the Chang'E-1 DTMs were interpolated from the relatively sparse Chang'E-1 LAM points and may not be sufficient to represent the actual topography in this area. Fig. 9 also shows obvious offsets between the profiles derived from the original Chang'E-1 DTMs (cyan lines) and the profiles from the LRO DTM (blue lines). After co-registration using the multi-feature-based method, the profiles derived from the co-registered Chang'E-1 DTM (red lines) are quite consistent with the LRO profiles for all the four reference lines as shown in Fig. 9(a), (c), (e) and (g). Although the profiles derived from the co-registered Chang'E-1 DTM using the point-based method (purple lines) are closer to the LRO profiles after co-registration, there are still obvious offsets between the profiles, as shown in Fig. 9(b), (d), (f) and (h).

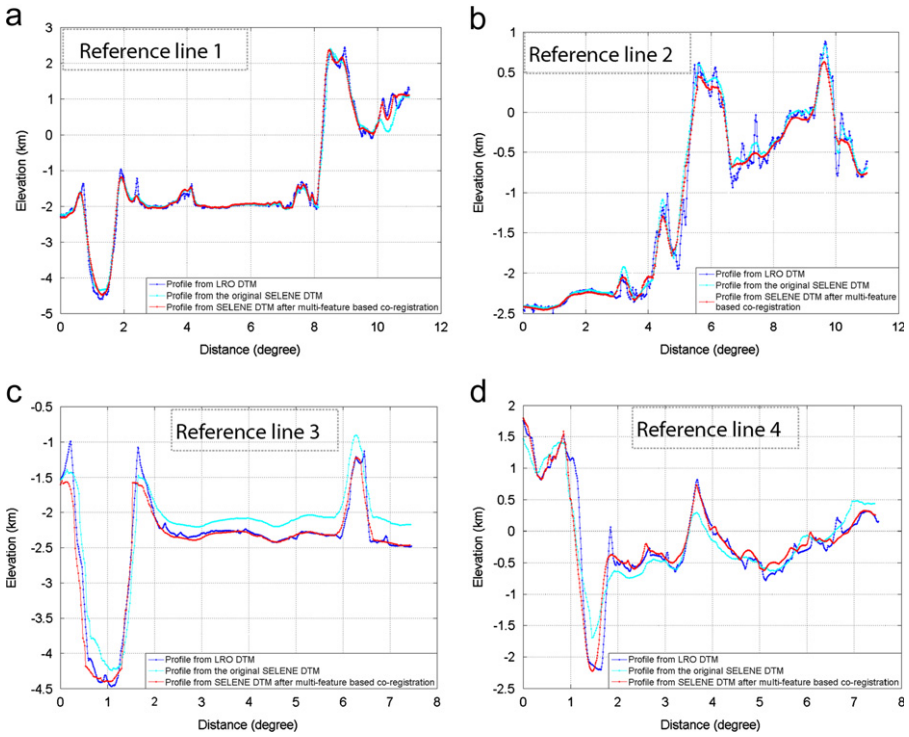

Fig. 10. Profiles derived from the LRO DTM, the original SELENE DTM, and the SELENE DTM after multi-feature based co-registration in the Apollo 15 landing area. (a) Profiles for reference line 1, (b) profiles for line 2, (c) profiles for line 3, and (d) profiles for line 4.

Table 4
Statistics of the absolute elevation differences between the profiles derived from the SELENE and LRO DTMs in the Apollo 15 landing area.

	Average	Maximum	Minimum	Standard deviation
	(m)	(m)	(m)	(m)
Reference line 1				
LRO profile–SELENE profile (original)	31.98	865.26	0.04	193.01
LRO profile–SELENE profile (multi-feature-based method)	7.67	652.89	0.01	138.38
Reference line 2				
LRO profile–SELENE profile (original)	40.22	818.99	0.04	136.99
LRO profile–SELENE profile (multi-feature-based method)	13.64	730.46	0.001	131.77
Reference line 3				
LRO profile–SELENE profile (original)	189.29	858.40	2.50	231.75
LRO profile–SELENE profile (multi-feature-based method)	48.35	673.30	0.00	142.97
Reference line 4				
LRO profile–SELENE profile (original)	91.57	1023.70	2.70	270.85
LRO profile–SELENE profile (multi-feature-based method)	2.55	848.40	0.50	169.67

The absolute elevation differences of the profiles were calculated and the statistics including the average, maximum, minimum, and standard deviation were obtained. They are shown in Table 2. The results indicate that the multi-feature-based co-registration method performed much better than the point-based method.

4.1.2. *Co-registration of SELENE and LRO DTMs in the Apollo 15 landing area*

Similar processes were used to co-register the DTM derived from the SELENE LALT data with the DTM derived from the LRO LOLA data in the Apollo 15 landing area. The results from the point-based co-registration method are omitted here. Table 3 lists the seven transformation parameters of the SELENE and LRO DTMs obtained using the multi-feature-based co-registration method. There is about a 40 m offset between the SELENE and LRO DTMs in the horizontal direction, and the SELENE data are generally about 164 m higher than the LRO data. The rotation deviations between the two datasets are small, and their scales are very similar.

Fig. 10 shows the profiles for the same four reference lines illustrated in Fig. 8, including profiles derived from the LRO DTM, the original SELENE DTM, and the SELENE DTM after multi-feature-based co-registration. Table 4 lists the statistics of the absolute elevation differences of these profiles.

Fig. 10 and Table 4 show that the SELENE and LRO profiles along the north–south direction are quite consistent. The averages of the absolute elevation differences between the profiles derived from the original SELENE DTM and LRO DTM are 31.98 m for reference line 1 and 40.22 m for line 2. For the profiles along the east–west direction (reference lines 3 and 4), the differences are much larger, showing

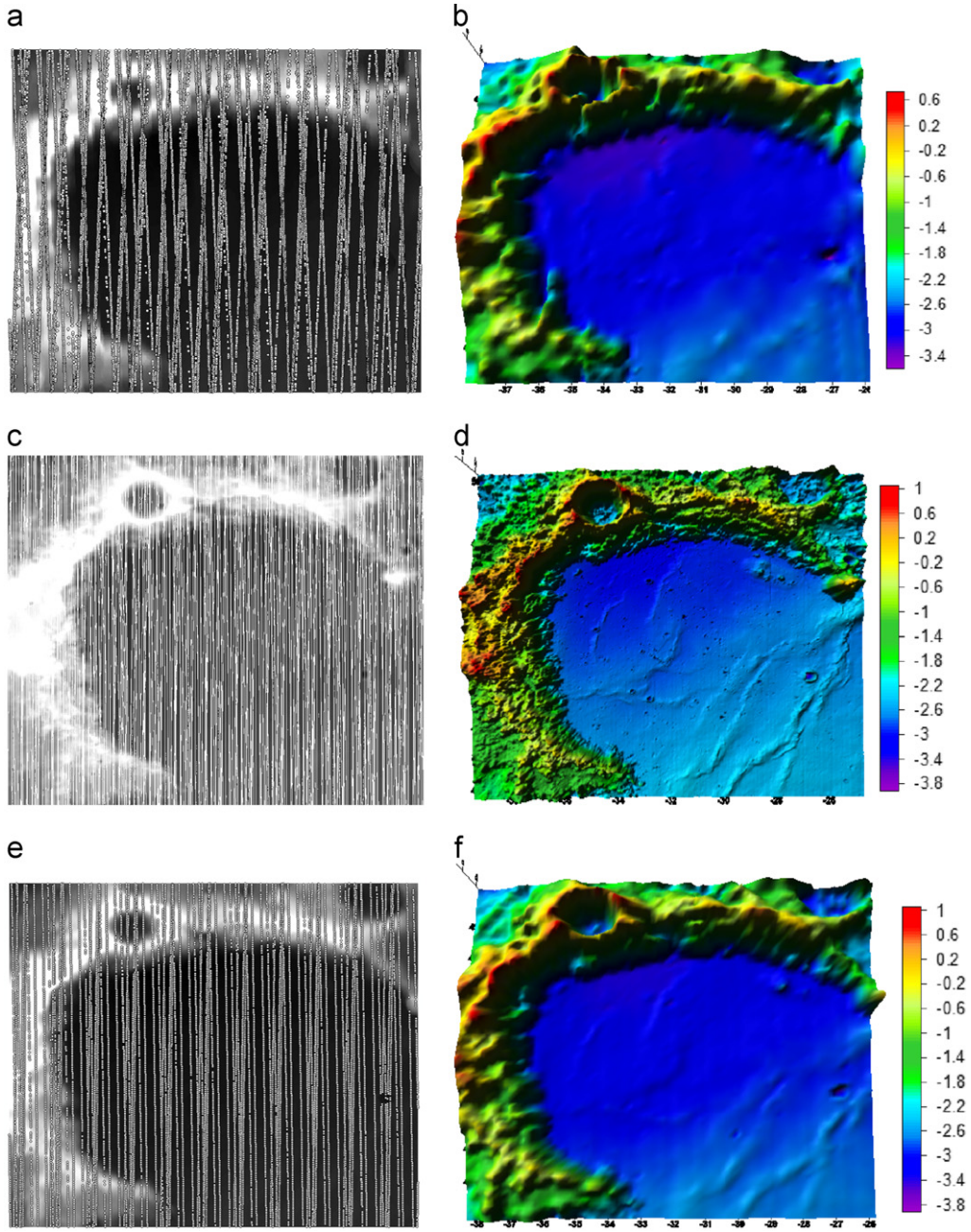

Fig. 11. Chang'E-1 LAM, SELENE LALT, and LRO LOLA data and DTMs in the Sinus Iridum area. (a) Chang'E-1 LAM data (15,581 points) overlaid on the DTM, (b) 3D view of the Chang'E-1 DTM, (c) LRO LOLA data (1,428,761 points) overlaid on the DTM, (d) 3D view of the LRO DTM, (e) SELENE LALT data (18,379 points) overlaid on the DTM and (f) 3D view of the SELENE DTM.

averages of 189.29 m for reference line 3 and 91.57 m for line 4. In comparing the profiles at reference line 3, it can be seen that the original SELENE data are clearly higher than the LRO data in the upper-right part of the study area. After applying multi-feature-based co-registration, the differences are reduced significantly for all four reference lines.

4.2. Co-registration of multiple lunar DTMs in the Sinus Iridum area

Sinus Iridum is a plain of basaltic lava that forms a north-western extension to the Mare Imbrium. The Chinese first lunar lander/rover Chang'E-3 is planned to land on the Sinus Iridum landing area in 2013. In this study, the Sinus Iridum area covered a region of 26–38°W and 40–50°N, including a large flat area surrounded by mountains. The maximum elevation difference is about 5 km. Fig. 11 shows the distributions of the laser altimeter points from Chang'E-1 LAM, LRO LOLA, and SELENE LALT at the study area. There were 15,581, 1,428,761, and 18,379 points from Chang'E-1 LAM, LRO LOLA, and SELENE LALT, respectively. DTMs with the same spatial resolution, 0.02° grid spacing (about 600 m in latitude and 400 m in longitude), were interpolated from the laser altimeter points, respectively. The points were overlaid on their corresponding DTMs as illustrated in Fig. 11(a), (c), and (e). Fig. 11(b), (d), and (f) show the 3D view of the DTMs.

4.2.1. Co-registration of Chang'E-1 and SELENE DTMs in the Sinus Iridum area

In the Sinus Iridum area, the developed multi-feature-based surface matching method was used to co-register the Chang'E-1

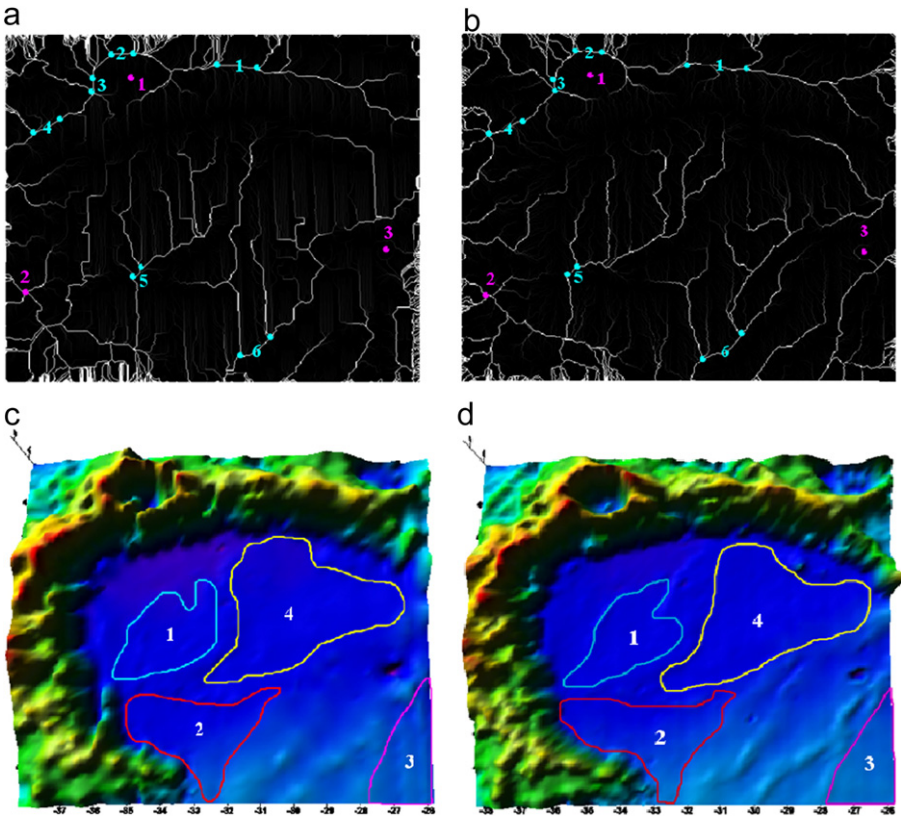

Fig. 12. Feature points, lines, and surface patches determined on the Chang'E-1and SELENE DTMs in the Sinus Iridum area. (a) The selected feature points (marked with purple) and line segments (cyan) on the Chang'E-1 DTM, (b) the corresponding feature points and line segments on the SELENE DTM, (c) the selected surface patches on the Chang'E-1 DTM and (d) the corresponding surface patches on the SELENE DTM.

Table 5
Transformation parameters between the Chang'E-1 and SELENE DTMs in the Sinus Iridum area.

Transformation parameters	Multi-feature-based method	Point-based method
Scale	1.0024	1.0027
ΔX (longitude)	−301.18 m	−403.69 m
ΔY (latitude)	−357.18 m	−380.80 m
ΔZ (altitude)	−230.91 m	−799.42 m
$\Delta\varphi$ (roll)	0.0073	0.022
$\Delta\omega$ (pitch)	0.0028	−0.0009
$\Delta\kappa$ (yaw)	−0.0072	−0.0095

DTM to the SELENE DTM. Three point pairs (two crater centers and one feature point) and six line pairs were identified from the two DTMs as illustrated in Fig. 12(a) and (b). Four pairs of surface patches were also identified from the two DTMs as shown in Fig. 12(c) and (d). They were then used as inputs in the adjustment model for surface matching.

After surface matching using the multi-feature-based method, seven transformation parameters were obtained. They are listed in Table 5. The results show that for the DTMs derived from the Chang'E-1 LAM and SELENE LALT data in the Sinus Iridum area, there were about 470 m offset between the two datasets in the horizontal direction, and the SELENE data were about 230 m higher than the Chang'E-1 data. The point-based surface matching method was also tested for the Chang'E-1 and SELENE DTMs in the Sinus Iridum area. Thirteen point pairs including the three used in the previous method were used, and the obtained transformation parameters are also listed in Table 5.

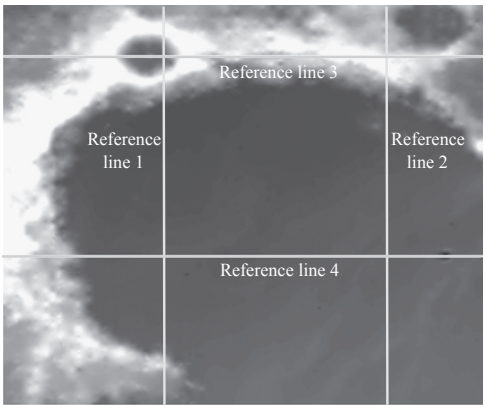

Fig. 13. Four reference lines selected for comparison analysis in the Sinus Iridum area.

The obtained transformation parameters were used to co-register the Chang'E-1 DTM to the SELENE DTM. To evaluate the performances of the co-registration method, four reference lines were selected for profile comparison analysis as shown in Fig. 13, of which lines 1 and 2 are along the north–south direction and lines 3 and 4 are along the east–west direction.

Three profiles were derived for each reference line, including a profile derived from the SELENE DTM, a profile interpolated from the original Chang'E-1 DTM, and a profile interpolated from the Chang'E-1 DTM after co-registering to the SELENE DTM. Fig. 14(a), (c), (e) and (g) show the results from the multi-feature-based co-registration, and Fig. 14(b), (d), (f) and (h) show the results from

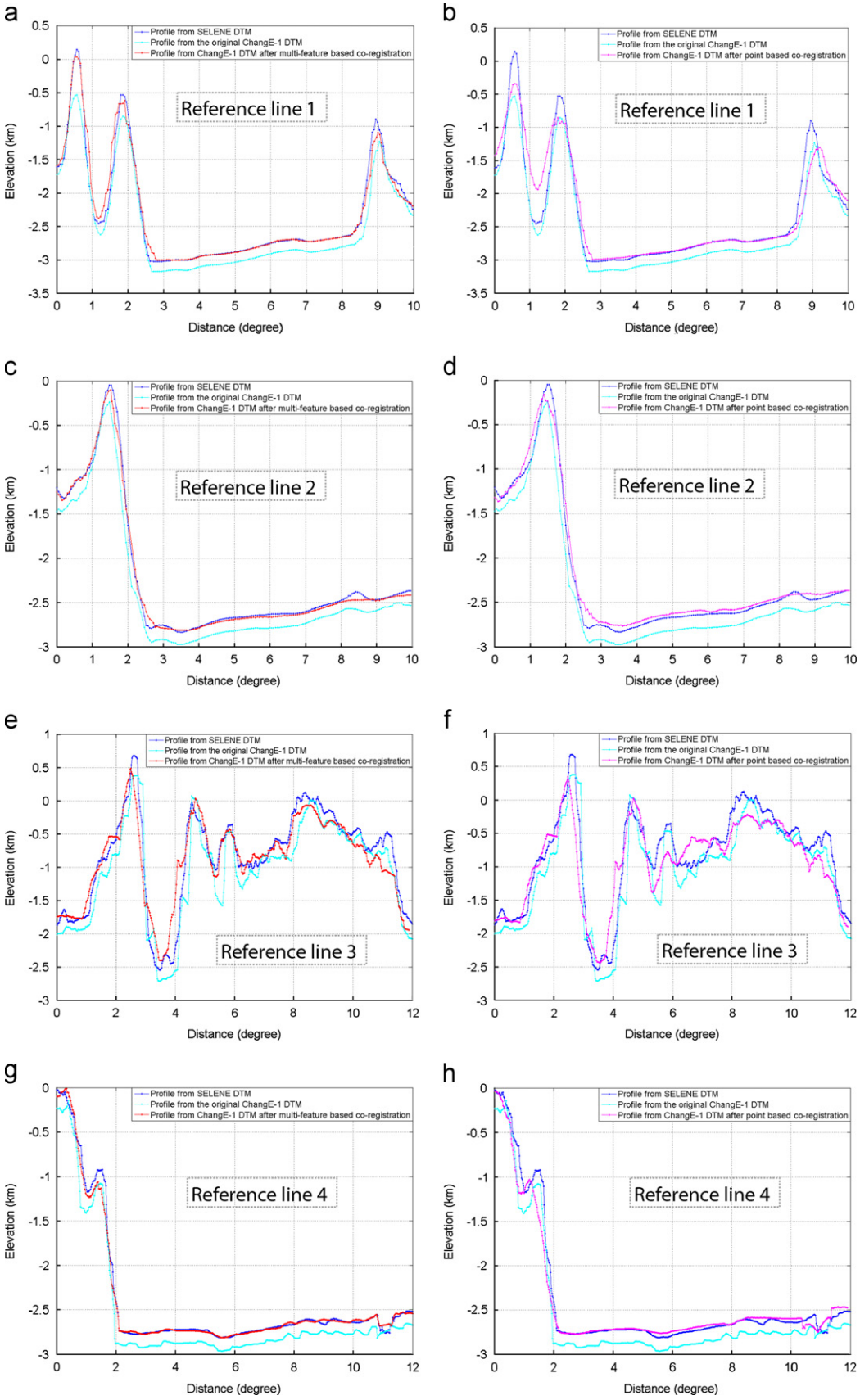

Fig. 14. Profiles derived from the SELENE and Chang'E-1 DTMs in the Sinus Iridum area. (a) Profiles for reference line 1 using multi-feature based co-registration, (b) profiles for line 1 using point based co-registration, (c) profiles for line 2 using multi-feature based co-registration, (d) profiles for line 2 using point based co-registration, (e) profiles for line 3 using multi-feature based co-registration, (f) profiles for line 3 using point based co-registration, (g) profiles for line 4 using multi-feature based co-registration and (h) profiles for line 4 using point based co-registration. (For interpretation of the references to color in this figure, the reader is referred to the web version of this article.)

Table 6
Statistics of the absolute elevation differences between the profiles derived from the Chang'E-1 and SELENE DTMs in the Sinus Iridum area.

	Average	Maximum	Minimum	Standard deviation
	(m)	(m)	(m)	(m)
Reference line 1				
SELENE profile–Chang'E-1 profile (original)	176.80	734.17	1.41	233.35
SELENE profile–Chang'E-1 profile (multi-feature-based method)	15.18	521.28	0.07	124.74
SELENE profile–Chang'E-1 profile (point-based method)	34.97	724.29	0.30	114.96
Reference line 2				
SELENE profile–Chang'E-1 profile (original)	154.78	520.44	2.02	74.17
SELENE profile–Chang'E-1 profile (multi-feature-based method)	15.72	276.47	0.91	68.16
SELENE profile–Chang'E-1 profile (point-based method)	39.76	256.97	0.24	49.38
Reference line 3				
SELENE profile–Chang'E-1 profile (original)	192.86	1244.5	0.60	300.26
SELENE profile–Chang'E-1 profile (multi-feature-based method)	29.76	1118.9	0.50	230.40
SELENE profile–Chang'E-1 profile (point-based method)	73.11	1152.70	0.70	255.05
Reference line 4				
SELENE profile–Chang'E-1 profile (original)	149.55	697.50	0.80	123.97
SELENE profile–Chang'E-1 profile (multi-feature-based method)	17.78	402.80	0.00	9.48
SELENE profile–Chang'E-1 profile (point-based method)	61.28	664.10	0.20	74.34

Table 7
Transformation parameters between the SELENE and LRO DTMs in the Sinus Iridum area.

Transformation parameters	Multi-feature-based method
Scale	0.9989
ΔX (longitude)	−22.87 m
ΔY (latitude)	51.42 m
ΔZ (altitude)	7.74 m
$\Delta\varphi$ (roll)	−0.0003°
$\Delta\omega$ (pitch)	0.00008°
$\Delta\kappa$ (yaw)	0.00014°

the point-based co-registration. Fig. 14 shows that the general trends among these profiles are consistent for all the four reference lines in this study area. There are obvious offsets between the profiles derived from the original Chang'E-1 DTMs (cyan lines) and the profiles from the SELENE DTMs (blue lines). After co-registration using the multi-feature-based method, the profiles derived from the co-registered Chang'E-1 DTM (red lines) are closely attached to the SELENE profiles for the four reference lines as shown in Fig. 14(a), (c), (e) and (g). Although the profiles derived from the co-registered Chang'E-1 DTM using the point-based method (purple lines) are closer to the SELENE profiles compared with the profiles before co-registration, there are still obvious offsets between the profiles, as shown in Fig. 14(b), (d), (f) and (h).

The absolute elevation differences of the profiles were calculated and the statistics are given in Table 6. The results show that the multi-feature-based co-registration method again performed better than the point-based method. The average absolute elevation differences were reduced significantly after using the multi-feature-based co-registration method.

4.2.2. Co-registration of SELENE and LRO DTMs in the Sinus Iridum area

Similar processes were performed to co-register the DTM derived from the SELENE LALT data with the DTM derived from the LRO LOLA data in the Sinus Iridum area. Table 7 lists the seven transformation parameters of the SELENE and LRO DTMs obtained using the multi-feature-based co-registration method. The results show that there are about 56 m offset between the SELENE and LRO DTMs in the horizontal direction, and the elevations of the two datasets are fairly consistent in the study area. The rotation deviations and scale differences between the two datasets are all very small.

Fig. 15 shows the profiles for the same four reference lines illustrated in Fig. 13, including profiles derived from the LRO DTM, the original SELENE DTM, and the SELENE DTM after multi-feature-based co-registration. Table 8 lists the statistics of the absolute elevation differences of these profiles.

Fig. 15 and Table 8 show that the profiles derived from the original SELENE DTM and LRO DTM are quite consistent. The averages of the absolute elevation differences between the profiles for all four reference lines are less than 10 m. The differences are further reduced for the profiles derived from the SELENE DTM after multi-feature-based co-registration. The obvious discrepancies in the right part of the profiles in Fig. 15(d) are because of the better resolution of the LRO LOLA data with respect to the SELENE LALT data when generating the DTMs.

As mentioned previously, one of the benefits of multiple DTM co-registration is the full synergistic use of multiple datasets and generation of consistent and better lunar topographic products. After the SELENE and Chang'E-1 DTMs were co-registered to the LRO DTM using the multi-feature-based method, the derived transformation parameters were used to bring the SELENE LALT and Chang'E-1 LAM datasets into alignment with the LRO LOLA. The DTMs with 0.01° grid spacing resolutions (about 300 m in latitude and 200 m in longitude) were generated using all of the laser altimeter points at the Apollo 15 landing area and the Sinus Iridum area. Fig. 16 shows a side-by-side visualization of the original DTMs derived from the LRO LOLA data and the new DTMs, indicating that the latter provides finer and more detailed topographic information. The yellow boxes marked in Fig. 16(b) and (d) show obvious examples.

5. Conclusions and discussion

This study presents a multi-feature-based surface matching method and applies it to the co-registration of multiple lunar DTMs derived from Chang'E-1, SELENE, and LRO laser altimeter data. The experimental analysis that used the datasets in the

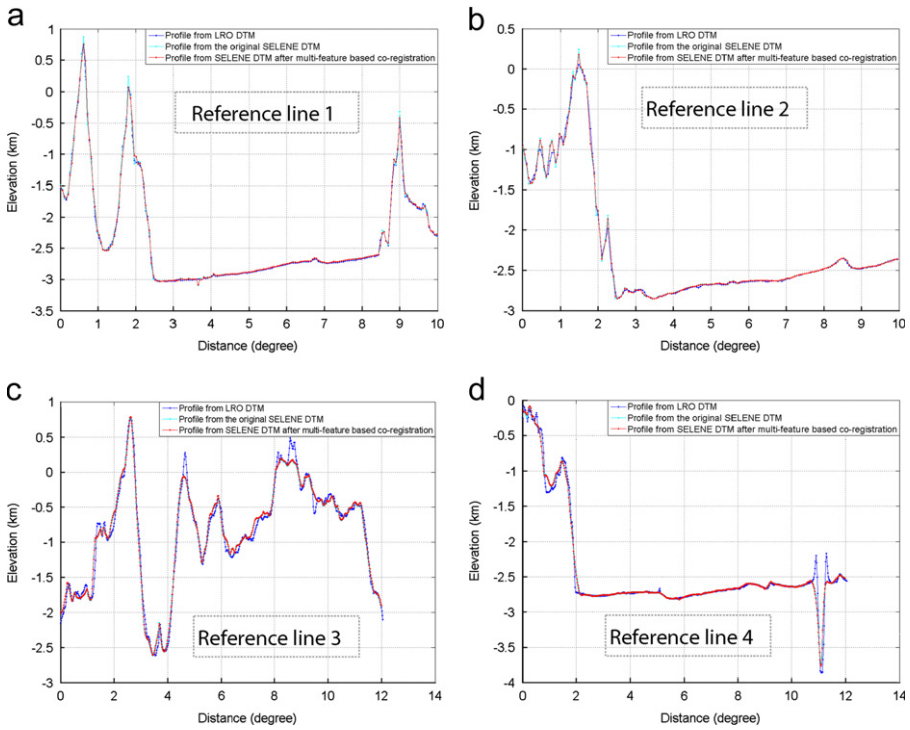

Fig. 15. Profiles derived from the LRO DTM, the original SELENE DTM, and the SELENE DTM after multi-feature based co-registration in the Sinus Iridum area. (a) Profiles for reference line 1, (b) profiles for line 2, (c) profiles for line 3, and (d) profiles for line 4.

Table 8
Statistics of the absolute elevation differences between the profiles derived from the SELENE and LRO DTMs in the Sinus Iridum area.

	Average	Maximum	Minimum	Standard deviation
	(m)	(m)	(m)	(m)
Reference line 1				
LRO profile–SELENE profile (original)	9.82	248.1	0.11	40.29
LRO profile–SELENE profile (multi-feature-based method)	9.66	170.58	0.08	35.19
Reference line 2				
LRO profile–SELENE profile (original)	5.41	199.87	0.11	41.34
LRO profile–SELENE profile (multi-feature-based method)	5.09	185.81	0.01	34.70
Reference line 3				
LRO profile–SELENE profile (original)	8.38	441.20	0.20	109.28
LRO profile–SELENE profile (multi-feature-based method)	1.65	413.50	0.20	93.90
Reference line 4				
LRO profile–SELENE profile (original)	1.44	670.3	0.00	98.28
LRO profile–SELENE profile (multi-feature-based method)	0.47	560.4	0.00	79.79

Apollo 15 landing area and the Sinus Iridum area leads to the following conclusions.

(1) In the Apollo 15 landing area, the LRO LOLA data are about 218 m higher than the Chang'E-1 LAM data, and there are about 25 m offset between the two datasets in the horizontal direction. For the SELENE LALT and LRO LOLA datasets, the SELENE data are generally about 164 m higher than the LRO data, and there are about 40 m offset between them in the horizontal direction. In the Sinus Iridum area, the SELENE LALT data are about 230 m higher than the Chang'E-1 LAM data, and there are about 470 m offset between them in the horizontal direction. There are about 56 m offset between the SELENE LALT and LRO LOLA datasets in the horizontal direction, and their elevations are fairly consistent in the study area.

(2) The multi-feature-based surface matching method is able to effectively co-register multiple lunar DTMs. After applying the co-registration method to the multiple DTMs, the differences among them could be significantly reduced in both the Apollo 15 landing area and the Sinus Iridum area. The multi-feature-based surface matching method performed much better than the point-based method.

The multi-feature-based surface matching method developed in this study was able to co-register multiple lunar DTMs derived from the data from different sensors in different missions to produce consistent and precise lunar topographic models. It could also be used to co-register other similar datasets. For example, it could be used to align LiDAR datasets and remove the offsets usually seen in adjacent LiDAR flight lines. It should be noted that the matching of feature points, lines, and surface patches must be done interactively in the current method. Future studies should

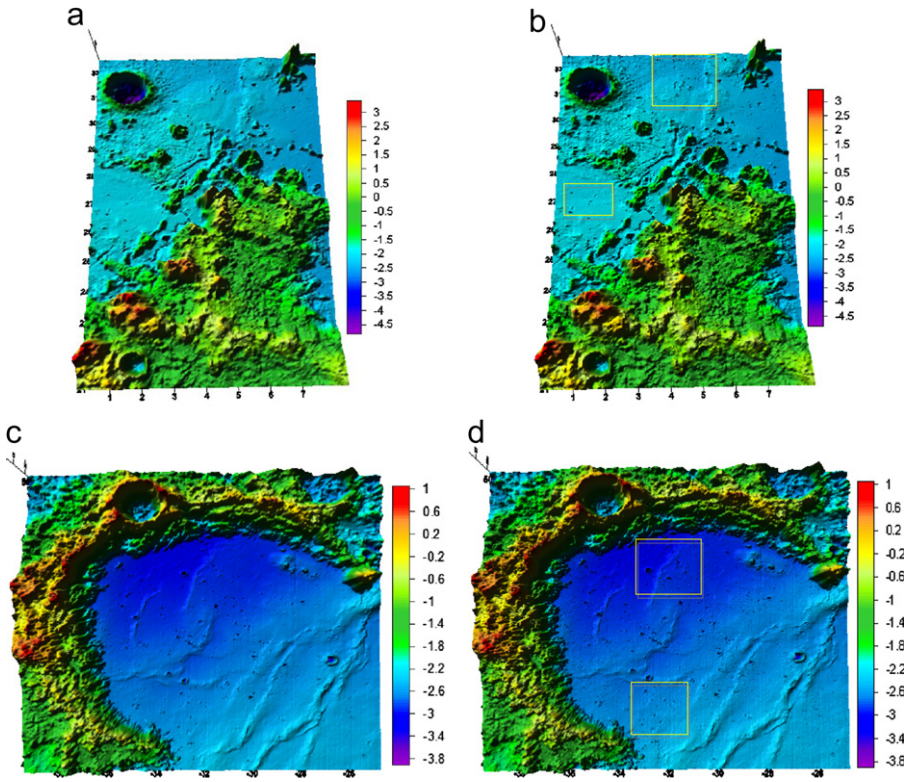

Fig. 16. Side by side visualization of the DTMs. (a) The original LOLA DTM in the Apollo 15 landing area, (b) the DTM derived by using all the aligned laser altimeter points in the Apollo 15 landing area, (c) the original LOLA DTM in the Sinus Iridum area, and (d) the DTM derived by using all the aligned laser altimeter points in the Sinus Iridum area. (For interpretation of the references to color in this figure, the reader is referred to the web version of this article.)

examine the automatic matching of these features so that the surface matching method can be fully automatic.

Acknowledgments

The authors would like to thank the National Astronomical Observatories of the Chinese Academy of Sciences for providing the Chang'E-1 datasets. The work described in this study was supported by a grant from the Research Grants Council of Hong Kong (Project no.: PolyU 5312/10E) and the Hong Kong Polytechnic University (Grant A/C 1-BB83). The work was also supported by a State 973 Project of China (#2012CB719901).

References

Anderson, F.S., Parker, T.J., 2002. Characterization of MER landing sites using MOC and MOLA. In: Proceedings of the 33rd Lunar and Planetary Science Conference, League City, Texas, March 11–15.

Araki, H., Tazawa, S., Noda, H., Ishihara, Y., Goossens, S., Sasaki, S., Kawano, N., Kamiya, I., Otake, H., Oberst, J., Shum, C., 2009. Lunar global shape and polar topography derived from Kaguya-LALT laser altimetry. Science 323, 897–900.

Archinal, B.A., Rosiek, M.R., Kirk, R.L., Redding, B.L., 2006. A Clementine derived control network and topographic model—the unified lunar control network 2005. In: Proceedings of the XXVIth IAU General Assembly, Session JD10, Prague, August 14–25, 2006.

Beyer, R.A., Archinal, B., Chen, Y., Edmundson, K., Harbour, D., Howington-Kraus, E., Li, R., McEwen, A., Mattson, S., Moratto, Z., Oberst, J., Rosiek, M., Scholten, F., Tran, T., Robinson, M., the LROC Team, 2010. LROC stereo data—results of initial analysis. In: Proceedings of the 41st Lunar and Planetary Science Conference, #2678.

Beyer, R.A., Archinal, B., Chen, Y., Edmundson, K., Howington-Kraus, E., Kirk, R., Li, R., McEwen, A., Mattson, S., Meng, X., Moratto, Z., Oberst, J., Rosiek, M., Scholten, F., Tran, T., Thomas, O., Wang, W., the LROC Team, 2011. LROC DTM comparison effort. In: Proceedings of the 42nd Lunar and Planetary Science Conference, #2715.

Besl, P., McKay, N., 1992. A method for registration of 3-D shapes. IEEE Trans. Pattern Anal. Mach. Intell. 14 (2), 239–256.

Burns, K.N., Speyerer, E.J., Robinson, M.S., Tran, T., Rosiek, M.R., Archinal, B.A., Howington-Kraus, E., the LROC Science Team, 2012. Digital Elevation Models and Derived Products from LROC NAC Stereo Observations. Int. Arch. Photogram. Remote Sensing Spat. Inf. Sci. XXXIX-B4, 483–488.

Chin, G., Brylow, S., Foote, M., Garvin, J., Kasper, J., Keller, J., Litvak, M., Mitrofanov, I., Paige, D., Raney, K., Robinson, M., Sanin, A., Smith, D., Spence, H., Spudis, P., Stern, S.A., Zuber, M., 2007. Lunar Reconnaissance Orbiter overview: the instrument suite and mission. Space Sci. Rev. 129, 391–419.

Di, K., Yue, Z., Peng, M., Liu, Z., 2010. Co-registration of Chang'E-1 stereo images and laser altimeter data for 3D mapping of lunar surface. In: Proceedings of a Special Joint Symposium of ISPRS Technical Commission IV & AutoCarto in conjunction with ASPRS/CaGIS 2010 Fall Specialty Conference, Orlando, FL, November 15–19.

Di, K., Liu, Y., Liu, B., Peng, M., 2012. Rigorous photogrammetric processing of Chang'E-1 and Chang'E-2 stereo imagery for lunar topographic mapping. Int. Arch. Photogram. Remote Sensing Spat. Inf. Sci. XXXIX-B4, 207–312.

Eliason, E., Isbell, C., Lee, E., Becker, T., Gaddis, L., McEwen, A., Robinson, M., 1999. Mission to the Moon: The Clementine UVVIS Global Lunar Mosaic. PDS Volumes USA_NASA_PDS_CL_4001 through 4078, Produced by the US Geological Survey and distributed on CD media by the Planetary Data System.

Garvin, J.B., S.E.H. Sakimoto, C. Schnetzler, J.J. Frawley, 1999. Global Geometric properties of martian impact craters: a preliminary assessment using Mars Orbiter Laser Altimeter (MOLA). In: Proceedings of the Fifth International Conference on Mars, July 18–23, Pasadena, CA.

Gruen, A., Akca, D., 2005. Least squares 3D surface matching. In: Proceedings of the ASPRS 2005 Annual Conference Geospatial Goes Global: From Your Neighborhood to the Whole Planet. Baltimore, Maryland, March 7–11.

Guo, J., Wu, B., 2012. Comparison analysis of lunar topographic models derived from Chang'E-1 and SELENE data. Int. Arch. Photogram. Remote Sensing Spat. Inf. Sci. XXXIX-B4, 313–319.

Haruyama, J., Hara, S., Hioki, K., Iwasaki, A., Morota, T., Ohtake, M., Matsunaga, T., Araki, H., Matsumoto, K., Ishihara, Y., Noda, H., Sasaki, S., Goossens, S., Iwata, T., 2012. Lunar global digital terrain model dataset produced from SELENE (Kaguya) terrain camera stereo observations. In: Proceedings of the Lunar and Planetary Science Conference, Woodlands, TX, March 19–23, LPS XLIII, 1200.

Kato, M., Sasakia, S., Tanakaa, K., Iijimaa, Y., Takizawaa, Y., 2008. The Japanese lunar mission SELENE: science goals and present status. Adv. Space Res. 42 (2), 294–300.

Kirk, R.L., Archinal, B.A., Gaddis, L.R., Rosiek, M.R., 2012. Lunar cartography: progress in the 2000s and prospects for the 2010s. Int. Arch. Photogram. Remote Sensing Spat. Inf. Sci. XXXIX-B4, 489–494.

Li, C.L., Ren, X., Liu, J., Zou, X., Mou, L., Wang, J., Shu, R., Zou, Y., Zhang, H., Lv, C., Liu, J., Zuo, W., Su, Y., Wen, W., Bian, W., Wang, M., Xu, C., Kong, D., Wang, X., Wang, F., Geng, L., Zhang, Z., Zheng, L., Zhu, X., Li, J., 2010a. Laser altimetry data of Chang'E-1 and the global lunar DEM model. Sci. China Earth Sci. 40 (3), 281–293.

Li, R., Wang, W., He, S., Hwangbo, J.W., Chen, Y., Tang, P., Meng, X., Choung, Y., Lawver, J., Thomas, P., Robinson, M., Rosiek, M., the LROC Team, 2010b. Precision photogrammetric modeling of LROC NAC cameras and topographic products. In: Proceedings of the Annual Meeting of the Lunar Exploration Analysis Group, Washington, DC, September 14–16, LPI Contribution no. 1595, p. 36.

Li, Z.L., Xu, Z., Chen, M., Ding, X.L., 2001. Robust surface matching for automated detection of local deformations using least-median-of-squares estimator. Photogram. Eng. Remote Sensing 67 (11), 1283–1292.

Lin, S.Y., Muller, J.P., Mills, J.P., Miller, P.E., 2010. An assessment of surface matching for the automated co-registration of MOLA, HRSC and HiRISE DTMs. Earth Planet. Sci. Lett. 294, 520–533.

Liu, J.J., Ren, X., Mu, L., Zhao, B., Xiang, B., Yang, J., Zou, Y., Zhang, H., Lu, C., Liu, J., Zuo, W., Su, Y., Wen, W., Bian, W., Zou, X., Li, C.L., 2009. Automatic DEM generation from Chang'E-1's CCD stereo camera images. In: Proceedings of the 40th Lunar and Planetary Science Conference, Houston, TX, March 23–27, 2570.

Livingston, R.G., 1980. Aerial cameras. In: Slama, C.C., Theurer, C., Henriksen, S.W. (Eds.), In Manual of Photogrammetry, 4th edition American Society of Photogrammetry and Remote Sensing, Falls Church, VA, pp. 187–278.

Mazarico, E., Rowlands, D., Neumann, G., Torrence, M., Smith, D., Zuber, M., 2011. Selenodesy with LRO: radio tracking and altimetric crossovers to improve orbit knowledge and gravity field estimation. In: Proceedings of the Lunar and Planetary Science Conference, Woodlands, TX, March 7–11, LPS XLII, 2215.

Mellberg, W.F., 1997. Moon Missions: Mankind's First Voyages to Another World. Plymouth Press, Ltd., Plymouth, MI.

Mikhail, E.M., Bethel, J.S., McGlone, J.C., 2001. Introduction to Modern Photogrammetry. John Wiley & Sons, Inc., p. 479.

Mills, J.P., Buckley, S.J., Mitchell, H.L., 2003. Synergistic fusion of GPS and photogrammetrically generated elevation models. Photogram. Eng. Remote Sensing 69 (4), 341–349.

Noda, H., Araki, H., Tazawa, S., Goossens, S., Ishihara, Y., the KAGUYA LALT Team, 2009. KAGUYA (SELENE) laser altimeter: one year in orbit. Geophysical Research Abstracts, 11, EGU2009-3841-1.

Ouyang, Z.Y., Li, C., Zou, Y., Zhang, H., Lv, C., Liu, J., Liu, J., Zuo, W., Su, Y., Wen, W., 2010. Preliminary scientific results of Chang'E-1 lunar orbiter. Sci. China 53 (11), 1565–1581.

Potts, L.V., von Frese, R.R.B., 2005. Impact-induced mass flow effects on lunar shape and the elevation dependence of nearside maria with longitude. Phys. Earth Planet. Inter. 153, 165–174.

Riris, H., Cavanaugh, J., Sun, X., Liiva, P., Rodriguez, M., Neuman, G., 2010. The Lunar Orbiter Laser Altimeter (LOLA) on NASA's Lunar Reconnaissance Orbiter (LRO) mission. In: Proceedings of the International Conference on Space Optics. Rhodes, Greece, October 4–8.

Robinson, M.S., Speyerer, E.J., Boyd, A., Waller, D., Wagner, R.V., Burns, K.N., 2012. Exploring the Moon with the Lunar Reconnaissance Orbiter camera. Int. Arch. Photogram. Remote Sensing Spat. Inf. Sci. XXXIX-B4, 501–504.

Rosiek, M., Kirk, R., Howington-Kraus, E., 1999. Lunar topographic maps derived from Clementine imagery. In: Proceedings of the Lunar and Planetary Science Conference, XXX Abstract #1853, LPI, Houston, TX, March 15–19.

Rosiek, M., Kirk, R., Hare, T., Howington-Kraus, E., 2001. Combining lunar photogrammetric topographic data with Clementine LIDAR data. In: Proceedings of the ISPRS WG IV/9: Extraterrestrial Mapping Workshop "Planetary Mapping 2001", Flagstaff, AZ, October 14–15.

Rosiek, M.R., Lee, E.M., Howington-Kraus, E.T., Fergason, R.L., Weller, L.A., Galuszka, D.M., Redding, B.L., Thomas, O.H., Saleh, R.A., Richie, J.O., Shinaman, J.R., Archinal, B.A., Hare, T.M., 2012. USGS digital terrain models and mosaics for LMMP. In: Proceedings of the 42nd Lunar and Planetary Science Conference, #2343.

Scholten, F., Oberst, J., Matz, K.-D., Roatsch, T., Wählisch, M., Speyerer, E.J., Robinson, M.S., 2012. GLD100: the near-global lunar 100 m raster DTM from LROC WAC stereo image data. J. Geophys. Res.—Planets 117, E00H17.

Smith, D.E., Zuber, M.T., Neumann, G.A., Lemoine, F.G., 1997. Topography of the Moon from the Clementine LiDAR. J. Geophys. Res.—Planets 102 (E1), 1591–1611.

Smith, D.E., Zuber, M.T., Jackson, G.B., Cavanaugh, J.F., Neumann, G.A., Riris, H., Sun, X., Zellar, R.S., Coltharp, C., Connelly, J., Katz, R.B., Kleyner, I., Liiva, P., Matuszeski, A., Mazarico, E.M., McGarry, J.F., Novo-Gradac, A., Ott, M.N., Peters, C., Ramos-Izquierdo, L.A., Ramsey, L., Rowlands, D.D., Schmidt, S., Scott, V.S., Shaw, G.B., Smith, J.C., Swinski, J., Torrence, M.H., Unger, G., Yu, A.W., Zagwodzki, T.W., 2010. The lunar orbiter laser altimeter investigation on the Lunar Reconnaissance Orbiter mission. Space Sci. Rev. 150 (1–4), 209–241.

Spiegel, M., 2007. Improvement of interior and exterior orientation of the three line camera HRSC with a simultaneous adjustment. Int. Arch. Photogram. Remote Sensing Spat. Inf. Sci. 36 (3/W49B), 161–166.

Streutker, D.R., Nancy, F.G., Shrestha, R., 2011. A slope-based method for matching elevation surfaces. Photogram. Eng. Remote Sensing 77 (7), 743–750.

Tarboton, D.G., 1997. A new method for the determination of flow directions and contributing areas in grid digital elevation models. Water Resour. Res. 33 (2), 309–319.

Tran, T., Rosiek, M., Ross, R., Beyer, A., Mattson, S., Howington-Kraus, E., Robinson, M.S., Archinal, B.A., Edmundson, K., Harbour, D., Anderson, E., the LROC Science Team, 2010. Generating digital terrain models using LROC NAC Images. In: Proceedings of the ASPRS/CaGIS 2010 Fall Specialty Conference, Orlando, Florida, November 15–19.

Waller, D.A., Boyd, A.K., Speyerer, E.J., Robinson, M.S., 2012. Constructing NAC polar maps that optimize lunar surface illumination. In: Proceedings of the Lunar and Planetary Science Conference, Woodlands, TX, March 19–23, LPS XLII, LPI Contribution No. 1659, id.2531.

Williams, J.A., Bennamoun, M., Latham, S., 1999. Multiple view 3D registration: a review and a new technique. In: Proceedings of the IEEE SMC'99 Conference, Tokyo, Japan, October 12–15.

Wu, B., Guo, J., Zhang, Y., King, B., Li, Z., Chen, Y., 2011. Integration of Chang'E-1 imagery and laser altimeter data for precision lunar topographic modeling. IEEE Trans. Geosci. Remote Sensing 49 (12), 4889–4903.

Yoon, J.-S., Shan, J., 2005. Combined adjustment of MOC stereo imagery and MOLA altimetry data. Photogram. Eng. Remote Sensing 71 (10), 1179–1186.

Zou, X.D., Liu, J.J., Mou, L.L., Ren, X., Li, K., Zhao, J.J., Liu, Y.X., Li, C.L., 2012. Topographic analysis of the proposed landing area of Sinus Iridum. EPSC Abstracts, 7, EPSC2012-151-1.